Check for updates

Geophysical Research Letters

RESEARCH LETTER
10.1029/2026GL124170

A Multi-Basin Calibration of Magnetofossils as a Quantitative Proxy for Bottom Water Oxygenation

Rong Huang[1], Liao Chang[1,2], Shengfa Liu[2,3], Jimin Yu[4,5], Wanyi Lu[6], Jianghui Du[1], Babette A. A. Hoogakker[7], Masanobu Yamamoto[8], Keiji Horikawa[9], Yuhji Yamamoto[10], Yusuke Okazaki[11], Pengfei Xue[6], Qishun Sun[1], Yanting Lin[1], Xuefa Shi[2,3], Somkiat Khokiattiwong[12], and Narumol Kornkanitnan[12]

[1]SKLab-DeepMinE, MOEKLab-OBCE, School of Earth and Space Sciences, Peking University, Beijing, China, [2]Laboratory for Marine Geology, Qingdao Marine Science and Technology Center, Qingdao, China, [3]Key Laboratory of Marine Geology and Metallogeny, First Institute of Oceanography, Ministry of Nature Resources, Qingdao, China, [4]Laoshan Laboratory, Qingdao, China, [5]Research School of Earth Sciences, Australian National University, Canberra, ACT, Australia, [6]State Key Laboratory of Marine Geology, Tongji University, Shanghai, China, [7]The Lyell Centre, Heriot-Watt University, Edinburgh, UK, [8]Faculty of Environmental Earth Science, Hokkaido University, Sapporo, Japan, [9]Faculty of Science, Academic Assembly, University of Toyama, Toyama, Japan, [10]Marine Core Research Institute, Kochi University, Kochi, Japan, [11]Department of Earth and Planetary Sciences, Graduate School of Science, Kyushu University, Fukuoka, Japan, [12]Marine and Coastal Resources Research and Development Institute, Department of Marine and Coastal Resources, Ministry of Natural Resources and Environment, Bangkok, Thailand

Key Points:

- Magnetofossil-based redox proxy is calibrated using 217 surface marine sediment samples across multiple basins
- Both magnetofossil coercivity fractions and crystal morphology linearly correlate with bottom-water oxygen concentrations (0–230 μmol/kg)
- Organic carbon primarily controls magnetofossil contents, with less influences on magnetofossil morphologies

Supporting Information:

Supporting Information may be found in the online version of this article.

Correspondence to:

L. Chang,
liao.chang@pku.edu.cn

Citation:

Huang, R., Chang, L., Liu, S., Yu, J., Lu, W., Du, J., et al. (2026). A Multi-basin calibration of magnetofossils as a quantitative proxy for bottom water oxygenation. *Geophysical Research Letters*, *53*, e2026GL124170. https://doi.org/10.1029/2026GL124170

Received 6 MAY 2026
Accepted 9 SEP 2026

© 2026 The Author(s). Geophysical Research Letters published by Wiley Periodicals LLC on behalf of American Geophysical Union.
This is an open access article under the terms of the Creative Commons Attribution License, which permits use, distribution and reproduction in any medium, provided the original work is properly cited.

Abstract

Magnetofossils, produced by magnetotactic bacteria, are widespread in marine sediments and are thought to be linked to oxygen concentrations. Until recently, their applications as a quantitative proxy for bottom water oxygen (BWO) are limited due to the lack of data from modern marine environments. Here, we present a multi-basin calibration of magnetofossil assemblages from a broad range of BWO concentrations using a large set of surface sediments. We find that both coercivity fractions and crystal morphologies of magnetofossils are linearly correlated with BWO over ~0–230 μmol/kg. We also find that while organic carbon contents primarily control magnetofossil abundance, it only has a weak influence on magnetofossil morphologies compared to BWO. Our calibration establishes magnetofossils as a quantitative oxygenation proxy, which provides rapid, and high-resolution reconstructions of past ocean oxygenation and associated deep-ocean carbon storage under climate transitions.

Plain Language Summary

Ocean oxygen plays a key role in regulating marine ecosystems and carbon cycles. However, quantitative reconstructions of past ocean oxygen concentrations remain challenging, particularly in well-oxygenated waters. Magnetofossils are remains of biological magnetite nanocrystals produced by magnetic bacteria, which are potential recorders of past ocean oxygenation. In this study, we find higher occurrence of bullet-shaped magnetofossils in low-oxygen environments, and cuboctahedral crystals are more abundant in well-oxygenated conditions. We have established a near global relationship between magnetofossil properties and ocean oxygen concentrations. These linear relationships allow the use of rapid magnetic measurements for quantifying past ocean oxygenation, providing valuable insights into investigating the oxygen and carbon cycles in Earth's history.

1. Introduction

Oceanic dissolved oxygen is a key component of the marine system, influencing ecological communities and biogeochemical cycles. Oxygen constrains the distribution and survival of most marine organisms, shaping marine biodiversity and ecosystem structure (Deutsch et al., 2015). In the surface ocean, oxygen is produced by photosynthesis, and is consumed in the ocean interior during the remineralization of sinking organic matter, therefore oxygen distributions are linked to the efficiency of the biological pump (Keeling et al., 2010). In addition, large-scale ocean overturning circulation controls oxygen distribution by ventilating ocean interior with oxygen-rich surface waters, thereby sustaining aerobic respiration in the deep sea (Talley, 2013). Consequently, dissolved oxygen integrates the combined effects of biological production, respiration, and ocean circulation (Keeling et al., 2010). Observations over recent decades show that the global ocean is undergoing notable deoxygenation (Breitburg et al., 2018; Schmidtko et al., 2017). However, instrumental records are too short to provide robust, longer-term context for ongoing climate change, and model simulations have considerable

19448007, 2026, 18, Downloaded from https://agupubs.onlinelibrary.wiley.com/doi/10.1029/2026GL124170 by Indian Institute Of Technology, Wiley Online Library on [27/09/2026]. See the Terms and Conditions (https://onlinelibrary.wiley.com/terms-and-conditions) on Wiley Online Library for rules of use; OA articles are governed by the applicable Creative Commons License

uncertainties (Kwiatkowski et al., 2020). Reconstructing past ocean oxygen variability is therefore essential for understanding the responses of Earth system to natural forcing and for improving predictions of future deoxygenation changes.

A variety of biological, geochemical, and sedimentological proxies have been developed to reconstruct past ocean oxygenation (Hoogakker et al., 2025). Each proxy has its strengths and limitations. Most proxies (e.g., sediment laminations, redox-sensitive trace metals) are qualitative indicators (Behl & Kennett, 1996; Morford & Emerson, 1999). A few proxies (e.g., benthic $\Delta\delta^{13}C$, benthic foraminiferal assemblages and morphology, foraminiferal I/Ca ratio, sedimentary U/Ba) allow for quantitative or semi-quantitative reconstructions (Costa et al., 2023; Dai & Yu, 2025; Hoogakker et al., 2015; Lu et al., 2020, 2022; Rathburn et al., 2018; Tetard et al., 2021, 2024). Among these, benthic $\Delta\delta^{13}C$ and sedimentary U/Ba are applicable across a relatively broad range (>50 μmol/kg), whereas most others are largely restricted to low-oxygen conditions (typically below 50 μmol/kg). The benthic $\Delta\delta^{13}C$ rely heavily on the preservation of foraminifera, making them inapplicable in the vast deep-sea regions below the carbonate compensation depth (CCD); whereas the sedimentary U/Ba proxy requires regional calibration (Costa et al., 2023; Costa & Oppo, 2026). At present, most marine basins have oxygen concentrations over 100 μmol/kg due to the high-latitude convection of oxygen-rich waters into the deep ocean (e.g., Dutkiewicz et al., 2015). Consequently, quantitative oxygen reconstruction in these high-oxygen and carbonate-poor environments remains challenging, highlighting the critical need for a globally applicable, quantitative oxygen proxy with a wide dynamic range.

Magnetotactic bacteria (MTB) commonly form magnetosomes which are composed of membrane-enclosed magnetite crystals (or less commonly greigite). This magnetite formation in MTB is highly sensitive to redox conditions influenced by oxygen concentrations (Ji et al., 2025; Jones et al., 2015; Kopp & Kirschvink, 2008; Lefèvre & Bazylinski, 2013; Wan et al., 2024). Under relatively oxic conditions, MTB producing cuboctahedral/octahedral particles are more abundant, whereas low-oxygen environments favor species that form elongated, particularly bullet-shaped magnetosomes (Ji et al., 2025). Consequently, the morphological assemblages and magnetic properties of magnetosomes preserved in sediments (called "magnetofossils", Kopp & Kirschvink, 2008) provide valuable information on past oxygen levels. Previous studies have qualitatively demonstrated the potential of magnetofossils as a BWO proxy (Blattman et al., 2020; Chang et al., 2018, 2023; Xue et al., 2022, 2023; Yamazaki et al., 2019). A recent work indicates a quantitative link between magnetofossil properties and ocean BWO concentrations in the Gulf of Alaska and South Atlantic (Xue, Chang, et al., 2025). However, due to the difficulty in separating magnetofossil signals through magnetic unmixing (Xue, Chang, et al., 2025), a comprehensive calibration spanning a wide oxygen range across multiple ocean basins is lacking, thus limiting the quantitative application of this proxy.

A widely used method for quantifying magnetofossil signals is the decomposition of isothermal remanent magnetization (IRM) acquisition curves based on the coercivity distributions of different magnetic minerals (Egli, 2004). Micromagnetic simulations indicate that magnetofossils can produce distinct magnetic components: elongated bullet-shaped magnetofossils predominantly contribute to the biogenic hard (BH) component, whereas equant cuboctahedral/octahedral particles mainly produce the biogenic soft (BS) component (Pei et al., 2023; Xue et al., 2024). The BH signal becomes detectable when the proportion of bullet-shaped grains exceeds ~2% (Xue et al., 2024). However, this method has ambiguities, as different choices in the number of components and parameter ranges can produce markedly different results, thereby affecting the quantification of magnetofossil signals. Transmission electron microscopy (TEM) observation provides critical constraints by directly identifying magnetic mineral assemblages and magnetofossil morphologies (e.g., Chang et al., 2018, 2023; Huang et al., 2025; Xue, Chang, et al., 2025; Xue et al., 2024). In addition, variations in magnetofossil assemblages are closely linked to oxygen levels and can provide independent evidence for BWO conditions. However, TEM is inefficient and expensive, thus it is generally applied only to representative samples to improve the robustness of magnetofossil quantification.

Here, we analyze 217 surface and core-top sediment samples from the Indian Ocean and Pacific Ocean (Figure 1, Text S1 in Supporting Information S1), in combination with published data, to establish a multi-basin quantitative relationship between BWO and magnetofossil properties, including magnetofossil coercivity fraction and crystal morphology fraction. All samples record near-modern or mid-late Holocene conditions (Figure S1, Text S2 in Supporting Information S1). The samples span both carbonate-rich and carbonate-barren sedimentary

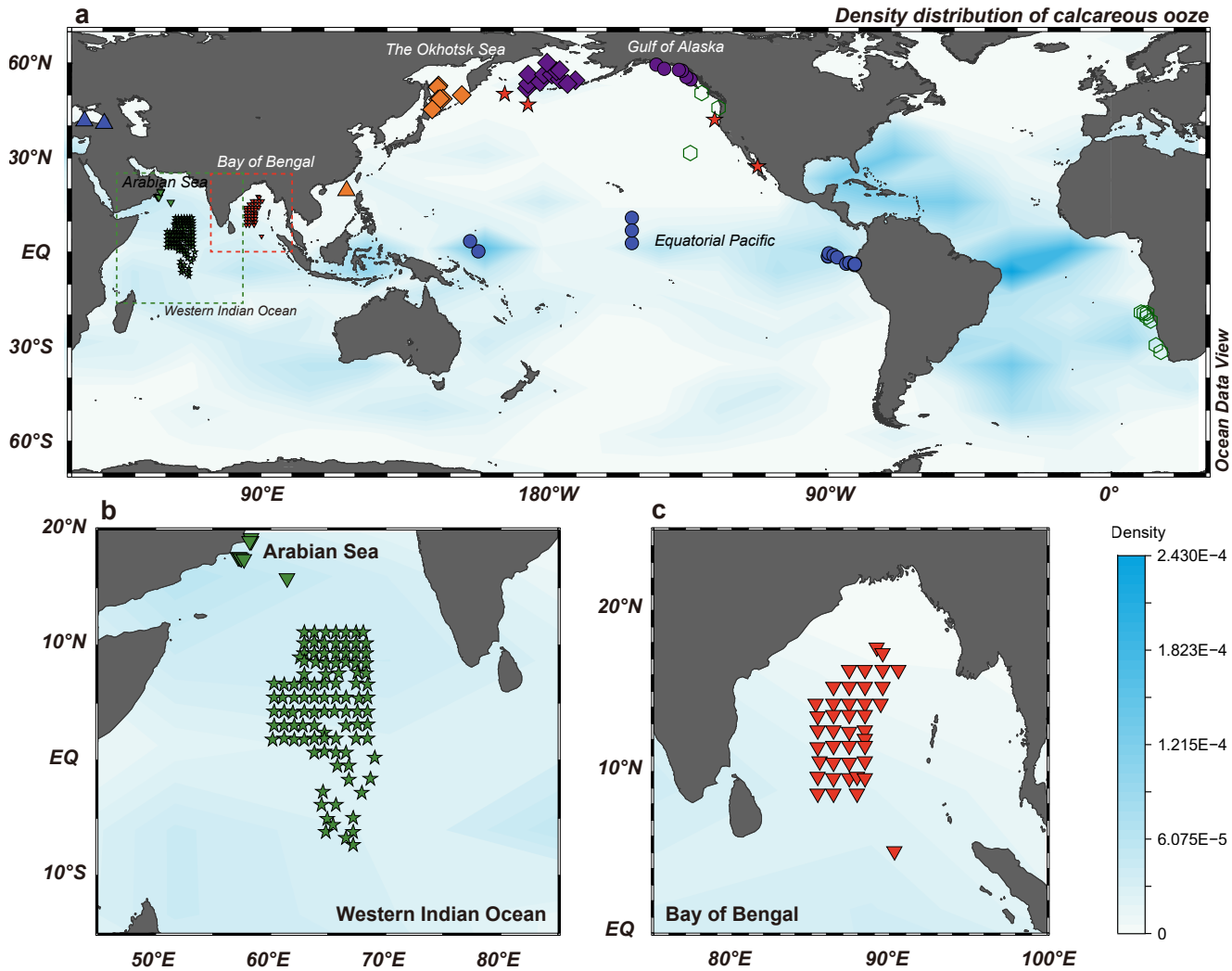


Figure 1. Sample locations. (a) Core sites are colored for different oceanographic areas. Sites from Xue et al. (2025) are shown in open hexagons. (b, c) Zoomed-in views of the Indian Ocean samples. Background shading shows the density distribution of calcareous ooze (data from Dutkiewicz et al., 2015). Darker blue corresponds to areas with a greater concentration of carbonate sediment occurrences. Maps were generated using Ocean Data View (Schlitzer, 2021).

environments, covering a broad oxygen range from 0 to 230 μmol/kg. We conducted systematic rock magnetic measurements and TEM observations (Text S3 in Supporting Information S1). More than 4,500 magnetofossil crystals were characterized. This integrated approach effectively reduces the ambiguities in the decomposition of mixed magnetic mineral signals from rock magnetic data, thereby enabling robust extraction of magnetofossil magnetic and morphological signals.

2. Quantifying Crystal Morphologies and Magnetic Properties of Magnetofossils

2.1. TEM Observations

To characterize magnetofossil morphological distributions, we analyzed a large number of magnetofossil crystals from eight representative samples (6 samples from the Indian Ocean and 2 from the Pacific) spanning a broad range of BWO concentrations (Figure S2, Tables S2 and S3 in Supporting Information S1). Magnetofossil crystals in all these samples are dominated by three main shapes: equant cuboctahedral/octahedral, elongated prismatic, and bullet-shaped morphologies (Figures 2a–2i). A total of 4,516 magnetofossil particles were identified and measured, with 299–1,160 particles counted per sample, providing robust statistical confidence of magnetofossil grain distributions and important constraints on magnetic unmixing of magnetofossil signals (Tables S2 and S3 in Supporting Information S1; Pei et al., 2022).

19448007, 2026, 18, Downloaded from https://agupubs.onlinelibrary.wiley.com/doi/10.1029/2026GL124170 by Indian Institute Of Technology, Wiley Online Library on [27/09/2026]. See the Terms and Conditions (https://onlinelibrary.wiley.com/terms-and-conditions) on Wiley Online Library for rules of use; OA articles are governed by the applicable Creative Commons License

10.1029/2026GL124170

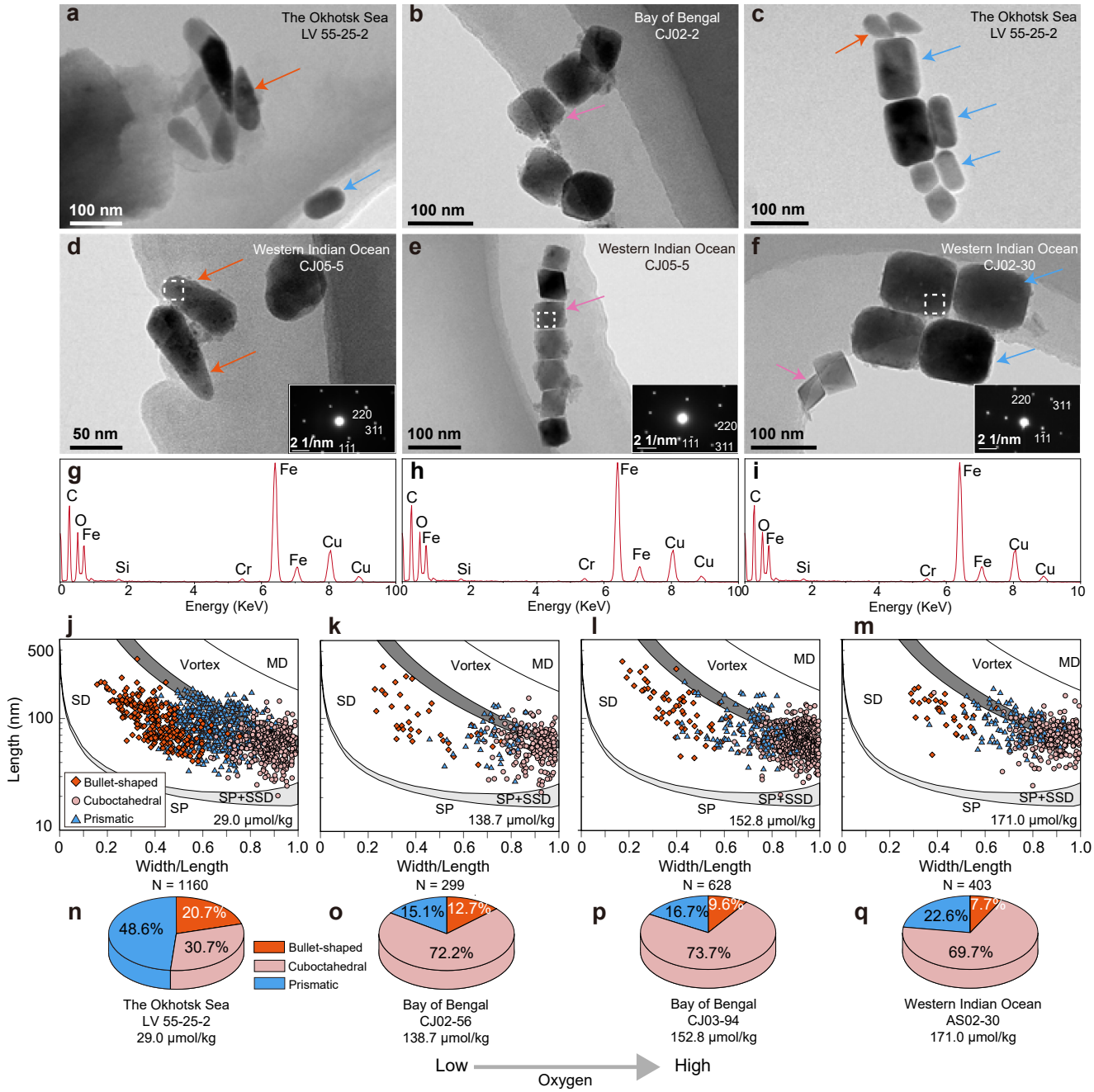


Figure 2. Transmission electron microscope (TEM) observations and statistical analyses of magnetofossil crystals of representative samples with increasing oxygen concentrations. (a–f) TEM images of different types of magnetofossil morphology (orange: bullet-shaped, blue: prismatic, pink: cuboctahedral/octahedral). (g–i) EDS spectra of particles in (d–f). Note that Cu is from the TEM grid. (j–m) Plotting of magnetofossil grain size distributions in the theoretical domain state phase diagram for samples (Muxworthy & Williams, 2009). (n–q) Pie chart of magnetofossil morphological content.

Identified magnetofossils predominantly fall within the single-domain range (Figures 2j–2m; Muxworthy & Williams, 2009). The relative proportions of magnetofossil morphologies vary systematically with BWO concentrations (Figures 2n–2q): bullet-shaped magnetofossils are abundant under low-oxygen environments and decrease with increasing oxygen concentrations, whereas cuboctahedral/octahedral particles show an opposite trend and become dominant in well-oxygenated conditions. Compared to bullet-shaped crystals, prismatic particles show a weaker relationship with oxygen levels, but are generally more abundant in low-oxygen conditions

19448007, 2026, 18, Downloaded from https://agupubs.onlinelibrary.wiley.com/doi/10.1029/2026GL124170 by Indian Institute Of Technology, Wiley Online Library on [27/09/2026]. See the Terms and Conditions (https://onlinelibrary.wiley.com/terms-and-conditions) on Wiley Online Library for rules of use; OA articles are governed by the applicable Creative Commons License

19448007, 2026, 18, Downloaded from https://agupubs.onlinelibrary.wiley.com/doi/10.1029/2026GL124170 by Indian Institute Of Technology, Wiley Online Library on [27/09/2026]. See the Terms and Conditions (https://onlinelibrary.wiley.com/terms-and-conditions) on Wiley Online Library for rules of use; OA articles are governed by the applicable Creative Commons License

(Table S3 in Supporting Information S1). These systematic morphological shifts indicate a strong oxygenation control on magnetofossil assemblages and provide direct support for their use as a quantitative indicator of BWO.

2.2. Magnetic Properties

Direct TEM identifications of magnetofossil occurrence provide key constraints on setting magnetofossil components in decomposing IRM curves. All IRM components were strictly constrained within physically reasonable parameter ranges to minimize ambiguities during the fitting procedures (Egli, 2004). The relative contributions of the BS and BH components were constrained using morphological statistics from direct TEM observations. Under these constraints, IRM acquisition curves were decomposed into distinct coercivity components corresponding to two magnetofossil populations (purple and cyan in Figures 3a–3d), and terrigenous detrital magnetite, maghemite, and hematite/goethite, respectively (blue, red, and green in Figures 3a–3d). The magnetofossil components show coercivities of 30.6–47.3 mT and 57.2–80.4 mT, with corresponding dispersion parameters (DP) of 0.164–0.238 and 0.123–0.221. These components are identified as BS (purple) and BH (cyan) magnetofossils, respectively (Chang et al., 2023; Egli, 2004; He & Pan, 2020; Lascu & Plank, 2013; Pei et al., 2023; Xue et al., 2024; Yamazaki et al., 2019). To quantify variations in magnetofossil magnetic signals, we calculated the BH fraction (δ_{BH}) as BH/(BH + BS). Samples from low-oxygen environments display high δ_{BH}, indicating a dominance of elongated magnetofossils (Figures 3a and 3b). In contrast, samples from more oxygenated conditions show markedly lower δ_{BH}, reflecting an increased contribution from more equant cuboctahedral/octahedral magnetofossils (Figures 3c and 3d).

First-order reversal curve (FORC) diagrams (Figures 3e–3h, Text S3 in Supporting Information S1) reveal similarly systematic variations as the IRM unmixing results (Figures 3a–3d). Single domain magnetofossils are characterized by a pronounced central-ridge FORC signature (Egli et al., 2010; Roberts et al., 2012). Samples from lower oxygen environments show FORC central ridges with higher peak coercivities (Figures 3e and 3f), consistent with the greater abundance of elongated magnetofossils with strong shape anisotropy. In contrast, well-oxygenated samples display much lower peak coercivities (Figures 3g and 3h), indicating a greater contribution from equant cuboctahedral/octahedral magnetofossil particles (Chang et al., 2023; Heslop et al., 2014; Pei et al., 2023).

Low-temperature magnetic measurements (Figures 3i–3l) further support these observations. Samples from low-oxygen environments show a pronounced Verwey transition (Verwey, 1939) at ∼100 K in the ZFC/FC warming curves (Figures 3i–3l), a characteristic feature of magnetofossils in marine sediments (Chang et al., 2016). With increasing oxygen concentrations, the Verwey transition gradually weakens and becomes negligible (Figures 3i–3l), suggesting enhanced oxidation of magnetofossil particles formed under more oxygenated conditions, which suppresses the Verwey transition signal (Özdemir et al., 1993).

3. Calibrations of Magnetic Signal and Morphology of Magnetofossils to BWO Concentration

Using all samples, we identified a strong negative correlation between δ_{BH} and BWO concentrations over a broad oxygen range (Figure 4a). The δ_{BH} decreases approximately with increasing BWO values, and can be described by a linear regression:

$$\delta_{BH} = -0.0014 \times BWO + 0.517 \left(R^2 = 0.86,\ p < 0.01\right).$$

This calibration applies over a range of oxygen concentration from 0 to 190 μmol/kg and is validated by Monte Carlo cross-validation and Spatial Leave-One-Out method (Text S4, Figures S3 and S4 in Supporting Information S1). These validation analyses demonstrate the robustness and spatial generalizability of the calibration, supporting its application across diverse marine settings. The uncertainties associated with reconstructing BWO are ±21 μmol/kg based on root mean-squared error. Here we also compared our results with the data set from Xue, Chang, et al. (2025). However, to avoid potential magnetic signal decomposition bias from high abundance of elongated prismatic grains, these magnetic data were excluded from our calibration curve (Text S5 in Supporting Information S1).

Because magnetofossil morphology represents a direct response to oxygenation conditions, we further evaluate morphological assemblages as quantitative oxygen indicators. Morphological data based on direct TEM

10.1029/2026GL124170

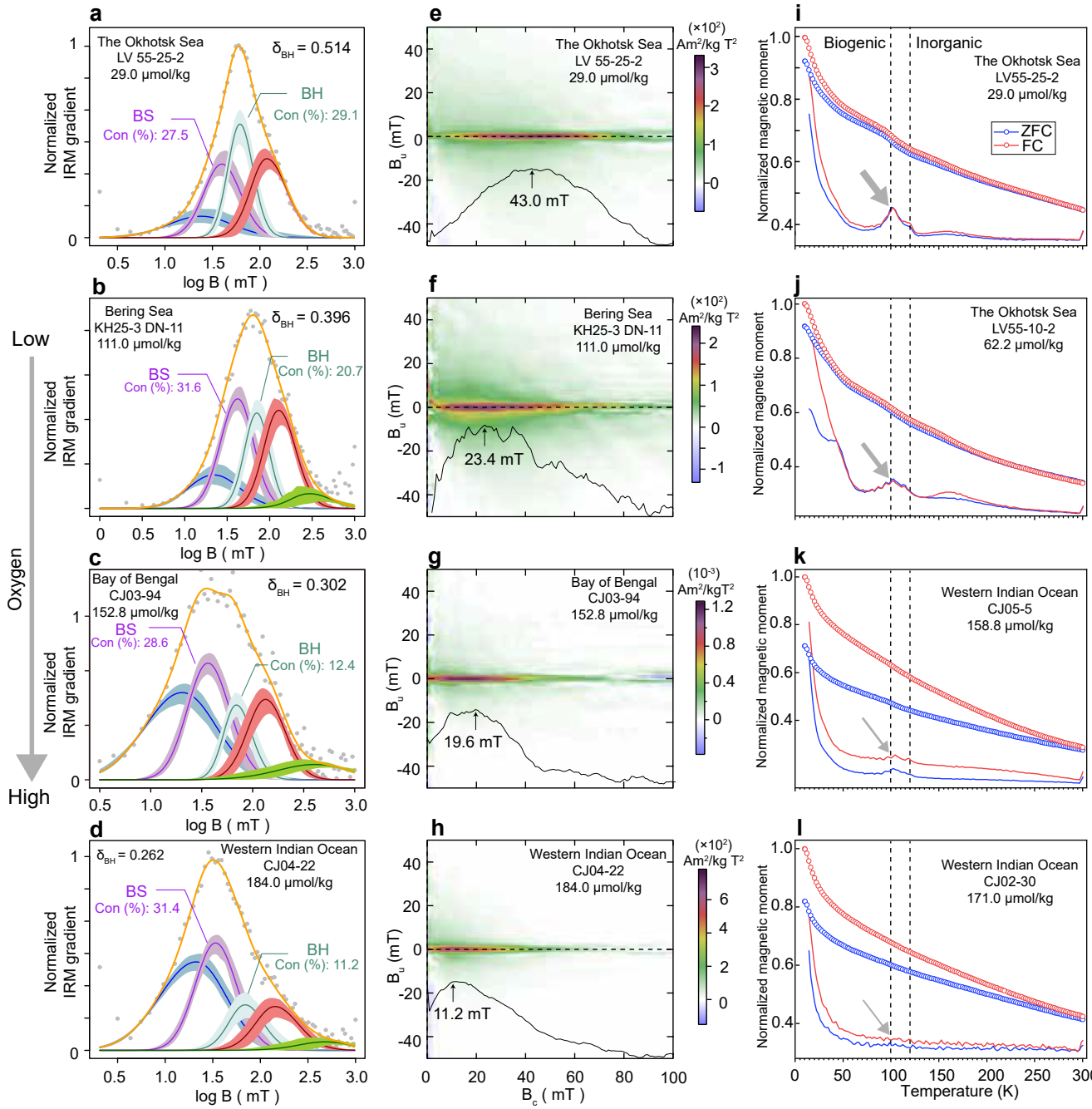


Figure 3. Magnetic properties of representative samples with progressively increasing oxygenation. (a–d) Decomposition of IRM acquisition curves using MAX UnMix (Maxbauer et al., 2016). Purple and cyan component represent biogenic soft (BS) and biogenic hard (BH) component, respectively. Blue, red and green represent detrital magnetite, maghemite, hematite/goethite. δ_{BH} and samples information are shown for each sample. (e–h) FORC diagrams and central ridge profiles (black lines) extracted by $|B_u| < 6$ mT. (i–l) Low-temperature magnetic properties. Remanence warming curves after zero-field (ZFC, blue circles) and field cooling (FC, red circles) and corresponding first-order derivative curves. Dashed lines and gray arrows indicate the temperature and strength of Verwey transitions (Verwey, 1939) of identified typical inorganic and biogenic magnetite sources in marine sediments (Chang et al., 2016).

observations from 8 representative samples in this study were combined with 16 published data sets to establish a global calibration (Figure S2, Tables S2 and S3 in Supporting Information S1; Huang et al., 2025; Usui & Yamazaki, 2021; Xue, Chang, et al., 2025; Yamazaki & Shimono, 2013; Yamazaki et al., 2019). Consistent with the magnetic calibration, magnetofossil morphology data quantitatively track BWO concentrations across a broad

19448007, 2026, 18, Downloaded from https://agupubs.onlinelibrary.wiley.com/doi/10.1029/2026GL124170 by Indian Institute Of Technology, Wiley Online Library on [27/09/2026]. See the Terms and Conditions (https://onlinelibrary.wiley.com/terms-and-conditions) on Wiley Online Library for rules of use; OA articles are governed by the applicable Creative Commons License

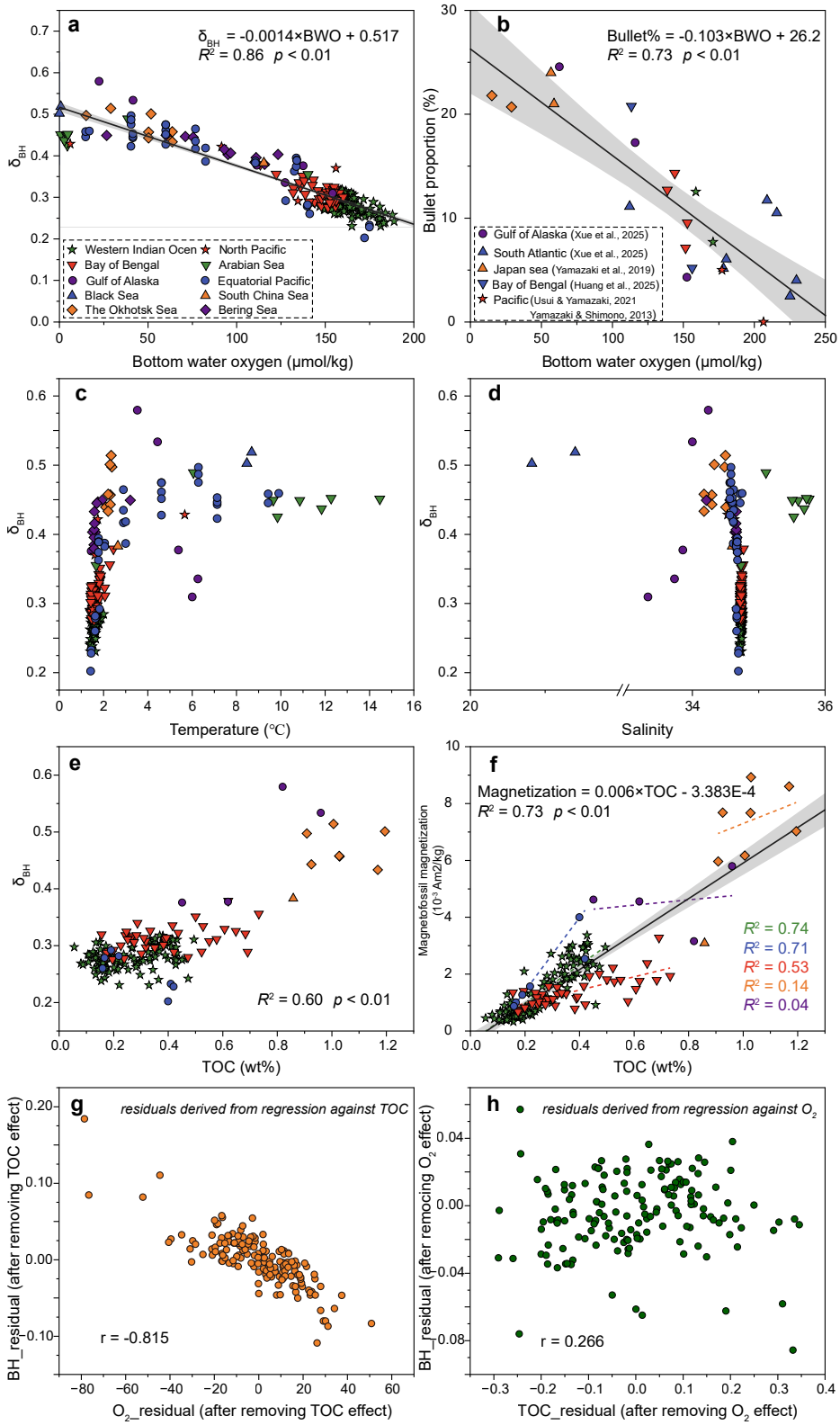


Figure 4.

19448007, 2026, 18, Downloaded from https://agupubs.onlinelibrary.wiley.com/doi/10.1029/2026GL124170 by Indian Institute Of Technology, Wiley Online Library on [27/09/2026]. See the Terms and Conditions (https://onlinelibrary.wiley.com/terms-and-conditions) on Wiley Online Library for rules of use; OA articles are governed by the applicable Creative Commons License

19448007, 2026, 18, Downloaded from https://agupubs.onlinelibrary.wiley.com/doi/10.1029/2026GL124170 by Indian Institute Of Technology, Wiley Online Library on [27/09/2026]. See the Terms and Conditions (https://onlinelibrary.wiley.com/terms-and-conditions) on Wiley Online Library for rules of use; OA articles are governed by the applicable Creative Commons License

oxygen range of 0–230 μmol/kg (Figure 4b, Figure S5 in Supporting Information S1). The proportion of bullet-shaped magnetofossils shows a strong negative correlation with BWO values, expressed as:

$$\text{Bullet}\% = -0.103 \times \text{BWO} + 26.2 \left(R^2 = 0.73,\ p\ <\ 0.01\right).$$

In contrast, the proportion of cuboctahedral/octahedral particles increases with oxygen concentration (Figure S5a in Supporting Information S1, $R^2 = 0.59$), whereas prismatic crystals show a weaker relationship (Figure S5b in Supporting Information S1, $R^2 = 0.37$). Therefore, the proportion of bullet-shaped magnetofossils provides the most robust quantitative indicator of BWO concentrations (Figure 4b). The proportion of bullet-shaped grains is also strongly correlated with the δ_{BH} (Figure S6 in Supporting Information S1, $R^2 = 0.73$), validating the calibration using magnetic properties. In addition to oxygen concentrations, we also investigate the influences of temperature and salinity on magnetofossils. No apparent correlation is observed (Figures 4c and 4d), suggesting that the magnetofossil signal is not controlled by these environmental factors.

4. Organic Carbon Controlling on Magnetofossil Abundance

Previous studies suggested that variations in magnetofossil morphological assemblages may be controlled by sedimentary total organic carbon (TOC) content (e.g., Yamazaki & Kawahata, 1998). Based on our results, TOC shows a moderately positive correlation with the δ_{BH} ($R^2 = 0.60$; Figure 4e). However, this relationship is significantly weaker than the correlation between δ_{BH} and oxygen concentrations ($R^2 = 0.86$; Figure 4a). Notably, TOC and BWO concentrations are also correlated ($R^2 = 0.60$; Figure S7 in Supporting Information S1), reflecting oxygen consumption during organic carbon respiration. This coupling complicates the interpretation of TOC's direct effects on the δ_{BH}.

To assess the relative controls of BWO versus TOC on the δ_{BH}, we conducted partial correlation coefficient analyses, which evaluates the relationship between two variables while controlling the influence of a third variable, thereby isolating their independent relationship (Text S6 in Supporting Information S1). After removing the influence of TOC, the δ_{BH} remains strongly correlated with BWO concentrations ($r = -0.815$; Figure 4g). In contrast, after removing the effect of BWO, the TOC and the δ_{BH} are almost uncorrelated ($r = 0.266$; Figure 4h). These results demonstrate that oxygen availability, rather than TOC content, might be the primary control on magnetofossil morphology, and therefore the δ_{BH}.

Although TOC shows a limited influence on magnetofossil morphology, it strongly controls magnetofossil abundance which is estimated by multiplying saturation IRM (SIRM) by the proportion of magnetofossil components (BH + BS). The magnetofossil abundance shows a significant positive linear relationship with TOC ($R^2 = 0.73$; Figure 4f). This relationship also shows clear regional variability likely due to different background environmental conditions, with steeper slopes in the western Indian Ocean ($R^2 = 0.74$) than in the Bay of Bengal ($R^2 = 0.53$), indicating higher rate of magnetofossil production under comparable TOC conditions.

Overall, these observations indicate a decoupling between environmental controls on magnetofossil abundance and morphology. TOC might primarily modulate the total biomass of MTB and thus magnetofossil abundance. In contrast, BWO concentration is the dominant control on magnetofossil morphology, which underpins the quantitative magnetofossil-based oxygen proxy using the δ_{BH}.

5. Magnetofossils as a Quantitative Redox Proxy and Implications

A full understanding of magnetofossil formation and preservation is essential for evaluating their application as quantitative oxygen proxies. Magnetofossils are intracellularly biomineralized magnetite produced by MTB. Many studies on lacustrine environments suggest that MTB predominantly inhabit the oxic–anoxic transition zone (OATZ; e.g., Bazylinski & Frankel, 2004; Ji et al., 2025; Moskowitz et al., 2008). However, in deep-sea

Figure 4. Calibration of magnetofossil-based proxy to BWO concentration and TOC controlling on magnetofossil assemblages. (a–b) Calibrations of magnetic signal and morphology proportion of magnetofossils to BWO concentrations. (c–d) Relations between δ_{BH} and temperature, δ_{BH} and salinity. (e–d) Relations between TOC and δ_{BH}, TOC and magnetofossil abundance. (g–h) Partial correlation coefficient analyses. (g) Relations between residuals of BWO concentrations and δ_{BH} after removing the influence of TOC, residuals of TOC and δ_{BH} after removing the influence of BWO concentrations. The Pearson correlation coefficient (r) is shown. High r value indicates strong correlation. The gray shaded band in all results indicates the 95% confidence interval.

19448007, 2026, 18, Downloaded from https://agupubs.onlinelibrary.wiley.com/doi/10.1029/2026GL124170 by Indian Institute Of Technology, Wiley Online Library on [27/09/2026]. See the Terms and Conditions (https://onlinelibrary.wiley.com/terms-and-conditions) on Wiley Online Library for rules of use; OA articles are governed by the applicable Creative Commons License

environments, low sedimentation rates and limited organic carbon burial result in highly variable OATZ depths, ranging from decimeters to over hundreds of meters below the seafloor. If marine MTB were restricted to the OATZ, magnetofossils would be almost absent from surface sediments in some deep-sea environments. However, our results reveal abundant magnetofossils even in topmost deep-sea surface sediments (Bering Sea and western Pacific). Abundant published data further support this observation (Huang et al., 2025; Liu et al., 2024; Xue, Chang, et al., 2025; Yamazaki et al., 2019; Yamazaki & Kawahata, 1998; Zhang & Wang, 2024). Yamazaki and Shimono (2013) reported the presence of magnetofossils even in oxidized red clay layers, which may suggest that MTB are not strictly confined to the OATZ and could, at least in some settings, occur within the upper few centimeters of surface sediment (Frankel et al., 1997; Li, Liu, Wang, et al., 2020; Petermann & Bleil, 1993). Integrating systematic magnetic and geochemical analyses, Blattmann et al. (2020) demonstrated that MTB distribution track changes in redox conditions associated with bottom-water oxygenation and the development of steep redox gradient at the sediment-water interface, rather than the deeper sediment pore water conditions. In addition, magnetofossil records almost always appear synchronous with climate variations, without significant temporal offset (Chang et al., 2023; Li et al., 2025; Xue et al., 2022; Yamazaki & Ikehara, 2012). These lines of evidence suggest that magnetofossils primarily record variations in bottom-water oxygenation rather than pore-water redox conditions.

Compared with existing (semi-)quantitative redox proxies, magnetofossils offer an independent approach for BWO reconstruction. Different proxies have distinct strengths and limitations depending on the depositional environment and oxygen range. For example, benthic foraminiferal porosity, I/Ca ratios, and $\Delta\delta^{13}C$, rely on the preservation of calcareous microfossils (Hoogakker et al., 2015; Lu et al., 2020, 2022; Rathburn et al., 2018). Benthic $\Delta\delta^{13}C$ is additionally influenced by anaerobic processes and methane hydrate release events within the sediments (Jacobel et al., 2020; Lu et al., 2022, 2026). Carbonate-based proxies cannot be applied below the CCD. In addition, many quantitative proxies are most sensitive under low-oxygen conditions (<50 μmol/kg), and therefore are primarily applicable within oxygen minimum zones (OMZs) (Lu et al., 2022). In contrast, MTB are widespread in marine environments, and are not restricted by carbonate preservation, making magnetofossils applicable in settings with rapid CCD changes (e.g., Palaeocene-Eocene Thermal Maximum; PETM). Our multi-basin calibration indicates that both magnetic signals and morphological assemblages of magnetofossils quantitatively track oxygen concentrations over at least 0–230 μmol/kg (Figures 4a and 4b), enabling reconstructions from OMZs to well-oxygenated deep oceans. Magnetic measurements are also rapid (~20 min per sample for coercivity spectra measurements), non-destructive, and performed directly on bulk sediments, facilitating efficient high-resolution oxygen reconstructions. These characteristics make magnetofossils a valuable complement to existing oxygenation proxies. Further calibration using additional core-top samples from open-ocean and low-productivity regions will help extend and refine the applicability of this proxy.

Although magnetofossil-based oxygenation proxy has advantages, limitations remain. The non-uniqueness of IRM unmixing is the primary problem. Since IRM unmixing is fundamentally a mathematical fitting procedure, the fit generally improves as more components are added in the fitting procedure. However, the result may not represent the true mineralogical assemblages. Additionally, some detrital magnetite can produce similar magnetic signals with magnetofossils, thereby complicating the IRM unmixing results. Therefore, TEM observation is essential to constrain IRM unmixing (Chang et al., 2018, 2019, 2023; Huang et al., 2025; Li, Liu, Liu, et al., 2020; Xue, Chang, et al., 2025; Xue, Huang, et al., 2025). TEM observations are more direct, but sample preparation and observations are relatively complex and labor-intensive. Magnetic extraction and counting magnetofossils are also time-consuming (e.g., Pei et al., 2022). The relatively higher analytical cost and inefficiency of TEM observations also make this unsuitable for high-resolution reconstructions. In addition, the calibration here should be applied to sediments without severe post-depositional reductive diagenesis, which can erase magnetofossil signals.

Overall, magnetofossils provide a new archive for quantitative reconstruction of BWO concentrations. Magnetofossil properties enable quantitative oxygen reconstructions in high-oxygen and non-calcareous deep-sea environments. It allows high-resolution oxygen reconstructions, which are essential for investigating rapid climate fluctuations (Sigman & Boyle, 2000). Furthermore, due to the close relationship between respired carbon and oxygen consumption (Anderson & Sarmiento, 1994), quantitative reconstructions of oxygen levels have important implications for understanding the dynamics of deep-ocean carbon storage and their role in regulating climate change.

6. Conclusion

Using a large set of surface marine sediments, we establish a multi-basin calibration of magnetofossils as a quantitative BWO proxy with a broad oxygen range. By integrating magnetofossil magnetic signals and morphological assemblages, we demonstrate strong linear relationships with BWO concentration. Our results further show that TOC primarily modulates magnetofossil abundance, and has less influence on magnetofossil morphologies than BWO concentrations. Compared with previous qualitative or semi-quantitative redox proxies, magnetofossils provide a complement proxy in both expanding applicability and measurement efficiency. Importantly, the magnetofossil proxy allows high-resolution quantitative reconstructions of BWO concentrations, thereby providing a useful means to investigate BWO variations and marine respired carbon storage during climate transitions.

Conflict of Interest

The authors declare no conflicts of interest relevant to this study.

Availability Statement

All data used in this study is available from Zenodo Repository (Huang et al., 2026) via the link: http://doi.org/10.5281/zenodo.20052566.

Acknowledgments
We thank 2014 and 2018 China-Thailand joint scientific cruises, the International Ocean Discovery Program, Marine and Geology Repository, Oregon State University, and Woods Hole Oceanographic Institute Seafloor Samples Repository for providing the surface and core-top samples. We thank Wenjing Qi, Bingjie Sun, and HuiHsin Wang for sampling assistance, Xu Tang for assistance with TEM analyses. We thank Toshitsugu Yamazaki and two anonymous reviewers for their helpful comments, and editor Monika Korte for editorial handling. This study is supported by the National Natural Science Foundation of China (NSFC) (Grants 42330204 to L.C. and B. A.A.H., 42525401 to L.C., 42476048 to W.L., 42330403 and W2511037 to J.Y.), the Scientific Research Innovation Capability Support Project for Young Faculty (SRICSPYF-ZY2025139) to W. L., the JSPS KAKENHI 25K22859 to K.H. and Y.O., the China Scholarship Council (202506010083) to R.H.

References

Anderson, L. A., & Sarmiento, J. L. (1994). Redfield ratios of remineralization determined by nutrient data analysis. *Global Biogeochemical Cycles*, *8*(1), 65–80. https://doi.org/10.1029/93GB03318

Bazylinski, D. A., & Frankel, R. B. (2004). Magnetosome formation in prokaryotes. *Nature Reviews Microbiology*, *2*(3), 217–230. https://doi.org/10.1038/nrmicro842

Behl, R., & Kennett, J. (1996). Brief interstadial events in the Santa Barbara basin, NE Pacific, during the past 60 kyr. *Nature*, *379*(6562), 243–246. https://doi.org/10.1038/379243a0

Blattmann, T. M., Lesniak, B., García-Rubio, I., Charilaou, M., Wessels, M., Eglinton, T. I., & Gehring, A. U. (2020). Ferromagnetic resonance of magnetite biominerals traces redox changes. *Earth and Planetary Science Letters*, *545*, 116400. https://doi.org/10.1016/j.epsl.2020.116400

Breitburg, D., Levin, L. A., Oschlies, A., Gregoire, M., Chavez, F. P., Conley, D. J., et al. (2018). Declining oxygen in the global ocean and coastal waters. *Science*, *359*(6371), eaam7240. https://doi.org/10.1126/science.aam7240

Chang, L., Harrison, R. J., & Berndt, T. A. (2019). Micromagnetic simulation of magnetofossils with realistic size and shape distributions: Linking magnetic proxies with nanoscale observations and implications for magnetofossil identification. *Earth and Planetary Science Letters*, *527*. https://doi.org/10.1016/j.epsl.2019.115790

Chang, L., Harrison, R. J., Zeng, F., Berndt, T. A., Roberts, A. P., Heslop, D., & Zhao, X. (2018). Coupled microbial bloom and oxygenation decline recorded by magnetofossils during the palaeocene–eocene thermal maximum. *Nature Communications*, *9*(1), 4007. https://doi.org/10.1038/s41467-018-06472-y

Chang, L., Heslop, D., Roberts, A. P., Rey, D., & Mohamed, K. J. (2016). Discrimination of biogenic and detrital magnetite through a double verwey transition temperature. *Journal of Geophysical Research: Solid Earth*, *121*(1), 3–14. https://doi.org/10.1002/2015jb012485

Chang, L., Hoogakker, B. A. A., Heslop, D., Zhao, X., Roberts, A. P., De Deckker, P., et al. (2023). Indian Ocean glacial deoxygenation and respired carbon accumulation during mid-late Quaternary ice ages. *Nature Communications*, *14*(1), 4841. https://doi.org/10.1038/s41467-023-40452-1

Costa, K. M., Nielsen, S. G., Wang, Y., Lu, W., Hines, S. K. V., Jacobel, A., & Oppo, D. W. (2023). Marine sedimentary uranium to barium ratios as a potential quantitative proxy for Pleistocene bottom water oxygen concentrations. *Geochimica et Cosmochimica Acta*, *343*, 1–16. https://doi.org/10.1029/2005PA001162

Costa, K. M., & Oppo, D. W. (2026). Controls on oxygen concentrations and δ13C in the glacial Atlantic. *Paleoceanography and Paleoclimatology*, *41*(1), e2025PA005222. https://doi.org/10.1029/2025PA005222

Dai, Y., & Yu, J. (2025). Contributions of biological and physical dynamics to deglacial CO_2 release from the polar Southern Ocean. *Nature Communications*, *16*(1), 2665. https://doi.org/10.1038/s41467-025-57677-x

Deutsch, C., Ferrel, A., Seibel, B., Pörtner, H.-O., & Huey, R. B. (2015). Climate change tightens a metabolic constraint on marine habitats. *Science*, *348*(6239), 1132–1135. https://doi.org/10.1126/science.aaa1605

Dutkiewicz, A., Müller, R. D., O'Callaghan, S., & Jónasson, H. (2015). Census of seafloor sediments in the world's ocean. *Geology*, *43*(9), 795–798. https://doi.org/10.1130/G36883.1

Egli, R. (2004). Characterization of individual rock magnetic components by analysis of remanence curves. *Physics and Chemistry of the Earth, Parts A/B/C*, *29*(13–14), 851–867. https://doi.org/10.1016/j.pce.2004.04.001

Egli, R., Chen, A. P., Winklhofer, M., Kodama, K. P., & Horng, C.-S. (2010). Detection of noninteracting single domain particles using first-order reversal curve diagrams. *Geochemistry, Geophysics, Geosystems*, *11*(1), Q01Z11. https://doi.org/10.1029/2009GC002916

Frankel, R. B., Bazylinski, D. A., Johnson, M. S., & Taylor, B. L. (1997). Magneto-aerotaxis in marine coccoid bacteria. *Biophysical Journal*, *73*(2), 994–1000. https://doi.org/10.1016/S0006-3495(97)78132-3

He, K., & Pan, Y. (2020). Magnetofossil abundance and diversity as paleoenvironmental proxies: A case study from southwest Iberian margin sediments. *Geophysical Research Letters*, *47*(8), e2020GL087165. https://doi.org/10.1029/2020GL087165

Heslop, D., Roberts, A. P., & Chang, L. (2014). Characterizing magnetofossils from first-order reversal curve (FORC) central ridge signatures. *Geochemistry, Geophysics, Geosystems*, *15*(6), 2170–2179. https://doi.org/10.1002/2014GC005291

Hoogakker, B. A. A., Davis, C., Wang, Y., Kusch, S., Nilsson-Kerr, K., Hardisty, D. S., et al. (2025). Reviews and syntheses: Review of proxies for low-oxygen paleoceanograpgic reconstructions. *Biogeosciences*, *22*(4), 863–957. https://doi.org/10.5194/bg-22-863-2025

19448007, 2026, 18, Downloaded from https://agupubs.onlinelibrary.wiley.com/doi/10.1029/2026GL124170 by Indian Institute Of Technology, Wiley Online Library on [27/09/2026]. See the Terms and Conditions (https://onlinelibrary.wiley.com/terms-and-conditions) on Wiley Online Library for rules of use; OA articles are governed by the applicable Creative Commons License

Hoogakker, B. A. A., Elderfield, H., Schmiedl, G., McCave, I. N., & Rickaby, R. E. M. (2015). Glacial–interglacial changes in bottom-water oxygen content on the Portuguese margin. *Nature Geoscience*, *8*(1), 40–43. https://doi.org/10.1038/ngeo2317

Huang, R., Chang, L., Liu, S., Yu, J., Lu, W., Du, J., et al. (2026). A multi-basin calibration of magnetofossils as a quantitative proxy for bottom water oxygenation [Dataset]. *Zenodo*. https://doi.org/10.5281/zenodo.20052566

Huang, R., Chang, L., Xue, P., Li, M., Liu, S., Shi, X., et al. (2025). Magnetofossil contribution to sedimentary magnetic records and sediment provenance reconstruction: A case from the bengal fan. *Journal of Geophysical Research: Solid Earth*, *130*(10), e2025JB031531. https://doi.org/10.1029/2025JB031531

Jacobel, A. W., Anderson, R. F., Jaccard, S. L., McManus, J. F., Pavia, F. J., & Winckler, G. (2020). Deep Pacific storage of respired carbon during the last ice age: Perspectives from bottom water oxygen reconstructions. *Quaternary Science Reviews*, *230*, 106065. https://doi.org/10.1016/j.quascirev.2019.106065

Ji, R., Wan, J., He, K., Goswami, P., Shen, J., Pan, Y., & Lin, W. (2025). Magnetosome gene cluster containing bacteria in oxygen-stratified freshwater ecosystems of northern landscapes. *Communications Earth & Environment*, *6*(1), 644. https://doi.org/10.1038/s43247-025-02495-8

Jones, S. R., Wilson, T. D., Brown, M. E., Rahn-Lee, L., Yu, Y., Fredriksen, L. L., et al. (2015). Genetic and biochemical investigations of the role of MamP in redox control of iron biomineralization in Magnetospirillum magneticum. *Proceedings of the National Academy of Sciences*, *112*(13), 3904–3909. https://doi.org/10.1073/pnas.1417614112

Keeling, R. F., Kortzinger, A., & Gruber, N. (2010). Ocean deoxygenation in a warming world. *Annual Review of Marine Science*, *2*(1), 199–229. https://doi.org/10.1146/annurev.marine.010908.163855

Kopp, R. E., & Kirschvink, J. L. (2008). The identification and biogeochemical interpretation of fossil magnetotactic bacteria. *Earth-Science Reviews*, *86*(1), 42–61. https://doi.org/10.1016/j.earscirev.2007.08.001

Kwiatkowski, L., Torres, O., Bopp, L., Aumont, O., Chamberlain, M., Christian, J. R., et al. (2020). Twenty-first century ocean warming, acidification, deoxygenation, and upper-ocean nutrient and primary production decline from CMIP6 model projections. *Biogeosciences*, *17*(13), 3439–3470. https://doi.org/10.5194/bg-17-3439-2020

Lascu, I., & Plank, C. (2013). A new dimension to sediment magnetism: Charting the spatial variability of magnetic properties across Lake basins. *Global and Planetary Change*, *110*, 340–349. https://doi.org/10.1016/j.gloplacha.2013.03.013

Lefèvre, C. T., & Bazylinski, D. A. (2013). Ecology, diversity, and evolution of magnetotactic bacteria. *Microbiology and Molecular Biology Reviews*, *77*(3), 497–526. https://doi.org/10.1128/mmbr.00021-13

Li, J., Liu, P., Wang, J., Roberts, A. P., & Pan, Y. (2020). Magnetotaxis as an adaptation to enable bacterial shuttling of microbial sulfur and sulfur cycling across aquatic oxic-anoxic interfaces. *Journal of Geophysical Research: Biogeosciences*, *125*(12), e2020JG006012. https://doi.org/10.1029/2020JG006012

Li, J., Liu, Y., Liu, S., Roberts, A. P., Pan, H., Xiao, T., & Pan, Y. (2020). Classification of a complexly mixed magnetic mineral assemblage in Pacific Ocean surface sediment by electron microscopy and supervised magnetic unmixing. *Frontiers in Earth Science*, *8*, 609058. https://doi.org/10.3389/feart.2020.609058

Li, Q., Li, Q., Chen, M.-T., Zhou, S., Zou, J., & Shi, X. (2025). Enhanced deoxygenation and carbon storage in the mid-depth subarctic Pacific during the Bølling-Allerød. *Earth and Planetary Science Letters*, *667*, 119529. https://doi.org/10.1016/j.epsl.2025.119529

Liu, Y., Liu, S., Piedrahita, V. A., Liu, P., He, S., Pan, H., et al. (2024). Insights into a correlation between magnetotactic bacteria and polymetallic nodule distribution in the eastern central Pacific Ocean. *Journal of Geophysical Research: Solid Earth*, *129*(8), e2024JB029062. https://doi.org/10.1029/2024jb029062

Lu, W., Oppo, D. W., Jiang, X., Dang, H., & Jian, Z. (2026a). Lower glacial oxygen in the eastern equatorial Pacific concentrated in the deep sea. *Geophysical Research Letters*, *53*(4), e2025GL119372. https://doi.org/10.1029/2025GL119372

Lu, W., Rickaby, R. E. M., Hoogakker, B. A. A., Rathburn, A. E., Burkett, A. M., Dickson, A. J., et al. (2020). I/Ca in epifaunal benthic foraminifera: A semi-quantitative proxy for bottom water oxygen in a multi-proxy compilation for glacial ocean deoxygenation. *Earth and Planetary Science Letters*, *533*, 116055. https://doi.org/10.1016/j.epsl.2019.116055

Lu, W., Wang, Y., Oppo, D. W., Nielsen, S. G., & Costa, K. M. (2022). Comparing paleo-oxygenation proxies (benthic foraminiferal surface porosity, I/Ca, authigenic uranium) on modern sediments and the glacial Arabian Sea. *Geochimica et Cosmochimica Acta*, *331*, 69–85. https://doi.org/10.1016/j.gca.2022.06.001

Maxbauer, D. P., Feinberg, J. M., & Fox, D. L. (2016). MAX UnMix: A web application for unmixing magnetic coercivity distributions. *Computers & Geosciences*, *95*, 140–145. https://doi.org/10.1016/j.cageo.2016.07.009

Morford, J. L., & Emerson, S. (1999). The geochemistry of redox sensitive trace metals in sediments. *Geochimica et Cosmochimica Acta*, *63*(11), 1735–1750. https://doi.org/10.1016/S0016-7037(99)00126-X

Moskowitz, B. M., Bazylinski, D. A., Egli, R., Frankel, R. B., & Edwards, K. J. (2008). Magnetic properties of marine magnetotactic bacteria in a seasonally stratified coastal pond (salt pond, MA, USA). *Geophysical Journal International*, *174*(1), 75–92. https://doi.org/10.1111/j.1365-246X.2008.03789.x

Muxworthy, A. R., & Williams, W. (2009). Critical superparamagnetic/single-domain grain sizes in interacting magnetite particles: Implications for magnetosome crystals. *Journal of the Royal Society Interface*, *6*(41), 1207–1212. https://doi.org/10.1098/rsif.2008.0462

Özdemir, Ö., Dunlop, D. J., & Moskowitz, B. M. (1993). The effect of oxidation on the verwey transition in magnetite. *Geophysical Research Letters*, *20*(16), 1671–1674. https://doi.org/10.1029/93GL01483

Pei, Z., Chang, L., Bai, F., & Harrison, R. J. (2023). Micromagnetic calculation of the magnetite magnetosomal morphology control of magnetism in magnetotactic bacteria. *Journal of the Royal Society Interface*, *20*(206), 20230297. https://doi.org/10.1098/rsif.2023.0297

Pei, Z., Chang, L., Xue, P., & Harrison, R. J. (2022). MagNet: Automated magnetic mineral grain morphometry using convolutional neural network. *Geophysical Research Letters*, *49*(12), e2022GL099118. https://doi.org/10.1029/2022gl099118

Petermann, H., & Bleil, U. (1993). Detection of live magnetotactic bacteria in south Atlantic deep-sea sediments. *Earth and Planetary Science Letters*, *117*(1), 223–228. https://doi.org/10.1016/0012-821X(93)90128-V

Rathburn, A. E., Willingham, J., Ziebis, W., Burkett, A. M., & Corliss, B. H. (2018). A new biological proxy for deep-sea paleo-oxygen: Pores of epifaunal benthic Foraminifera. *Scientific Reports*, *8*(1), 9456. https://doi.org/10.1038/s41598-018-27793-4

Roberts, A. P., Chang, L., Heslop, D., Florindo, F., & Larrasoaña, J. C. (2012). Searching for single domain magnetite in the "pseudo-single-domain" sedimentary haystack: Implications of biogenic magnetite preservation for sediment magnetism and relative paleointensity determinations. *Journal of Geophysical Research*, *117*(B8), B08104. https://doi.org/10.1029/2012JB009412

Schlitzer, R. (2021). Ocean data view. https://odv.awi.de

Schmidtko, S., Stramma, L., & Visbeck, M. (2017). Decline in global oceanic oxygen content during the past five decades. *Nature*, *542*(7641), 335–339. https://doi.org/10.1038/nature21399

19448007, 2026, 18, Downloaded from https://agupubs.onlinelibrary.wiley.com/doi/10.1029/2026GL124170 by Indian Institute Of Technology, Wiley Online Library on [27/09/2026]. See the Terms and Conditions (https://onlinelibrary.wiley.com/terms-and-conditions) on Wiley Online Library for rules of use; OA articles are governed by the applicable Creative Commons License

Sigman, D. M., & Boyle, E. A. (2000). Glacial/interglacial variations in atmospheric carbon dioxide. *Nature*, *407*(6806), 859–869. https://doi.org/10.1038/35038000

Talley, L. (2013). Closure of the global overturning circulation through the Indian, Pacific, and southern oceans: Schematics and transports. *Oceanography*, *26*(1), 80–97. https://doi.org/10.5670/oceanog.2013.07

Tetard, M., Licari, L., Ovsepyan, E., Tachikawa, K., & Beaufort, L. (2021). Toward a global calibration for quantifying past oxygenation in oxygen minimun zones using benthic foraminifera. *Biogeosciences*, *18*(9), 2827–2841. https://doi.org/10.5194/bg-18-2827-2021

Tetard, M., Prebble, J. G., & Cortese, G. (2024). Dissolved oxygen affinities of hundreds of benthic foraminiferal species. *Marine Micropaleontology*, *190*, 102380. https://doi.org/10.1016/J.MARMICRO.2024.102380

Usui, Y., & Yamazaki, T. (2021). Magnetostratigraphic evidence for post-depositional distortion of osmium isotopic records in pelagic clay and its implications for mineral flux estimates. *Earth Planets and Space*, *73*(1), 2. https://doi.org/10.1186/s40623-020-01338-4

Verwey, E. J. W. (1939). Electronic conduction of magnetite (Fe3O4) and its transition point at low temperatures. *Nature*, *144*(3642), 327–328. https://doi.org/10.1038/144327b0

Wan, J., Ji, R., Liu, J., Ma, K., Pan, Y., & Lin, W. (2024). Biomineralization in magnetotactic bacteria: From diversity to molecular discovery-based applications. *Cell Reports*, *43*(12), 114995. https://doi.org/10.1016/j.celrep.2024.114995

Wang, Y., Lu, W., Costa, K. M., & Nielsen, S. G. (2022). Beyond anoxia: Exploring sedimentary thallium isotopes in paleo-redox reconstructions from a new core top collection. *Geochimica et Cosmochimica Acta*, *333*, 347–361. https://doi.org/10.1016/j.gca.2022.07.022

Xue, P., Chang, L., Dickens, G. R., & Thomas, E. (2022). A depth-transect of ocean deoxygenation during the paleocene-eocene thermal maximum: Magnetofossils in sediment cores from the southeast Atlantic. *Journal of Geophysical Research: Solid Earth*, *127*(8), e2022JB024714. https://doi.org/10.1029/2022jb024714

Xue, P., Chang, L., Huang, R., Hoogakker, B. A. A., & Yi, L. (2025). Toward calibrating for bottom water oxygenation using magnetofossils: New insights from southeast Atlantic and northeast Pacific surface sediments. *Geophysical Research Letters*, *52*(20), e2025GL118127. https://doi.org/10.1029/2025GL118127

Xue, P., Chang, L., Pei, Z., & Harrison, R. J. (2024). The origin of magnetofossil coercivity components: Constraints from coupled experimental observations and micromagnetic calculations. *Journal of Geophysical Research: Solid Earth*, *129*(10), e2023JB028501. https://doi.org/10.1029/2023JB028501

Xue, P., Chang, L., & Thomas, E. (2023). Abrupt northwest Atlantic deep-sea oxygenation decline preceded the palaeocene-eocene thermal maximum. *Earth and Planetary Science Letters*, *618*, 118304. https://doi.org/10.1016/j.epsl.2023.118304

Yamazaki, T., & Ikehara, M. (2012). Origin of magnetic mineral concentration variation in the Southern Ocean. *Paleoceanography*, *27*(2), PA2206. https://doi.org/10.1029/2011pa002271

Yamazaki, T., & Kawahata, H. (1998). Organic carbon flux controls the morphology of magnetofossils in marine sediments. *Geology*, *26*(12), 1064–1066. https://doi.org/10.1130/0091-7613(1998)026<1064:OCFCTM>2.3.CO;2

Yamazaki, T., & Shimono, T. (2013). Abundant bacterial magnetite occurrence in oxic red clay. *Geology*, *41*(11), 1191–1194. https://doi.org/10.1130/g34782.1

Yamazaki, T., Suzuki, Y., Kouduka, M., & Kawamura, N. (2019). Dependence of bacterial magnetosome morphology on chemical conditions in deep-sea sediments. *Earth and Planetary Science Letters*, *513*, 135–143. https://doi.org/10.1016/j.epsl.2019.02.015

Zhang, X., & Wang, Y. (2024). Formation and preservation mechanisms of magnetofossils in the surface sediments of muddy areas in the yellow and bohai seas, China. *Marine Geology*, *477*, 107401. https://doi.org/10.1016/j.margeo.2024.107401

References From the Supporting Information

Arthur, M. A., & Dean, W. E. (1998). Organic-matter production and preservation and evolution of anoxia in the Holocene black sea. *Paleoceanography*, *13*(4), 395–411. https://doi.org/10.1029/98PA01161

Berger, W. H., Yasuda, M. K., Bickert, T., Wefer, G., & Takayama, T. (1994). Quaternary time scale for the ontong java Plateau: Milankovitch template for ocean drilling program site 806. *Geology*, *22*(5), 463–467. https://doi.org/10.1130/0091-7613(1994)022<0463:QTSFTO>2.3.CO;2

Bova, S. C., Herbert, T. D., & Altabet, M. A. (2018). Ventilation of northern and southern sources of aged carbon in the eastern equatorial Pacific during the younger dryas rise in atmospheric CO2. *Paleoceanography and Paleoclimatology*, *33*(11), 1151–1168. https://doi.org/10.1029/2018PA003386

Chauhan, O. Past 20,000-year history of Himalayan aridity: Evidence from oxygen isotope records in the Bay of Bengal.

Chen, L., Zhou, L., Liu, J., Yin, Z., Zhang, J., Guan, Y., et al. (2023). A stacked record of relative palaeointensity for past 500 ka from western equatorial Indian Ocean sediments. *Geophysical Journal International*, *235*(3), 2540–2555. https://doi.org/10.1093/gji/ggad383

De, S., & Singh, S. K. (2026). NADW attenuation and millennial-scale overturning circulation variability in the Arabian Sea constrained through authigenic εNd at the carlsberg ridge. *Geochimica et Cosmochimica Acta*, *423*, 176–194. https://doi.org/10.1016/j.gca.2026.04.048

Egli, R. (2013). VARIFORC: An optimized protocol for calculating non-regular first-order reversal curve (FORC) diagrams. *Global and Planetary Change*, *110*, 302–320. https://doi.org/10.1016/j.gloplacha.2013.08.003

Fang, T., Liu, S., Wu, K., Zhang, H., Cao, P., Huang, M., et al. (2024). Sediment provenance variations driven by sea level in the eastern Arabian Sea since the MIS 9 period: Evidence from geochemical proxies. *Journal of Asian Earth Sciences*, *266*, 106121. https://doi.org/10.1016/j.jseaes.2024.106121

Garcia, H. E., Weathers, K., Paver, C. R., Smolyar, I., Boyer, T. P., Locarnini, R. A., et al. (2019). *World Ocean Atlas 2018, volume 3: Dissolved oxygen, apparent oxygen utilization, and oxygen saturation* (Vol. 3). NOAA Atlas NESDIS.83.

Harrison, R. J., & Feinberg, J. M. (2008). FORCinel: An improved algorithm for calculating first-order reversal curve distributions using locally weighted regression smoothing. *Geochemistry, Geophysics, Geosystems*, *9*(5). https://doi.org/10.1029/2008gc001987

Jacobel, A. W., McManus, J. F., Anderson, R. F., & Winckler, G. (2017). Climate-related response of dust flux to the central equatorial Pacific over the past 150 kyr. *Earth and Planetary Science Letters*, *457*, 160–172. https://doi.org/10.1016/j.epsl.2016.09.042

Kiefer, T., Sarnthein, M., Erlenkeuser, H., Grootes, P. M., & Roberts, A. P. (2001). North Pacific response to millennial-scale changes in ocean circulation over the last 60 kyr. *Paleoceanography*, *16*(2), 179–189. https://doi.org/10.1029/2000PA000545

Kuehn, H., Lembke-Jene, L., Gersonde, R., Esper, O., Lamy, F., Arz, H., et al. (2014). Laminated sediments in the Bering Sea reveal atmospheric teleconnections to Greenland climate on millennial to decadal timescales during the last deglaciation. *Climate of the Past*, *10*(6), 2215–2236. https://doi.org/10.5194/cp-10-2215-2014

Li, J., Liu, S., Shi, X., Chen, M.-T., Zhang, H., Zhu, A., et al. (2020). Provenance of terrigenous sediments in the central Bay of Bengal and its relationship to climate changes since 25 ka. *Progress in Earth and Planetary Science*, *7*(1), 16. https://doi.org/10.1186/s40645-020-00328-0

19448007, 2026, 18, Downloaded from https://agupubs.onlinelibrary.wiley.com/doi/10.1029/2026GL124170 by Indian Institute Of Technology, Wiley Online Library on [27/09/2026]. See the Terms and Conditions (https://onlinelibrary.wiley.com/terms-and-conditions) on Wiley Online Library for rules of use; OA articles are governed by the applicable Creative Commons License

Li, J., Liu, S., Shi, X., Zhang, H., Fang, X., Chen, M.-T., et al. (2018). Clay minerals and Sr-Nd isotopic composition of the Bay of Bengal sediments: Implications for sediment provenance and climate control since 40 ka. *Quaternary International*, *493*, 50–58. https://doi.org/10.1016/j.quaint.2018.06.044

Liu, J., He, W., Cao, L., Zhu, Z., Xiang, R., Li, T., et al. (2019). Staged fine-grained sediment supply from the himalayas to the bengal fan in response to climate change over the past 50,000 years. *Quaternary Science Reviews*, *212*, 164–177. https://doi.org/10.1016/j.quascirev.2019.04.008

Liu, S., Ye, W., Zhang, H., Cao, P., Li, J., Sun, X., et al. (2023). Sediment provenances shift driven by sea level and Indian monsoon in the southern Bay of Bengal since the last glacial maximum. *Frontiers in Marine Science*, *10*, 1106663. https://doi.org/10.3389/fmars.2023.1106663

Lu, W., Costa, K. M., & Oppo, D. W. (2023). Reconstructing the oxygen depth profile in the Arabian Sea during the last glacial period. *Paleoceanography and Paleoclimatology*, *38*(6), e2023PA004632. https://doi.org/10.1029/2023pa004632

Lyle, M., Mix, A., Ravelo, A. C., Andreasen, D., Heusser, L., & Olivarez, A. (2000). Millennial-scale CaCO3 and C_{org} events along the northern and central California margin: Stratigraphy and origins. *Proceeding of the Ocean Drilling Program, Scientific Results*, *167*, 163–182. https://doi.org/10.2973/odp.proc.sr.167.214.2000

Lyle, M., Mix, A., & Pisias, N. (2002). Patterns of CaCO3 deposition in the eastern tropical Pacific Ocean for the last 150 kyr: Evidence for a southeast Pacific depositional spike during marine isotope stage (MIS) 2. *Paleoceanography*, *17*(2). https://doi.org/10.1029/2000PA000538

Macharia, R., & Manceau. (2026). Evolution of the hydrography of the Bay of Bengal over the last 500,000 years: An integrated approach combining modern planktonic Foraminifera ecology with fossil geochemical signatures. *Publication Number 2026ANGE0005) Université d'Angers*. Retrieved from https://theses.hal.science/tel-05637070

Naik, S. S., Basak, C., Goldstein, S. L., Naidu, P. D., & Naik, S. N. (2019). A 16-kyr record of ocean circulation and monsoon intensification from the central Bay of Bengal. *Geochemistry, Geophysics, Geosystems*, *20*(2), 872–882. https://doi.org/10.1029/2018gc007860

Nambiar, R., Bhushan, R., & Raj, H. (2022). Paleoredox conditions of bottom water in the northern Indian Ocean since 39 ka. *Palaeogeography, Palaeoclimatology, Palaeoecology*, *586*, 110766. https://doi.org/10.1016/j.palaeo.2021.110766

Okada, M., Takagi, M., Narita, H., & Takahashi, K. (2005). Chronostratigraphy of sediment cores from the Bering Sea and the subarctic Pacific based on paleomagnetic and oxygen isotopic analyses. *Deep Sea Research Part II: Topical Studies in Oceanography*, *52*(16), 2092–2109. https://doi.org/10.1016/j.dsr2.2005.08.004

Olsen, A., Key, R. M., van Heuven, S., Lauvset, S. K., Velo, A., Lin, X., et al. (2016). The global ocean data analysis project version 2 (GLODAPv2) – An internally consistent data product for the world ocean. *Earth System Science Data*, *8*(2), 297–323. https://doi.org/10.5194/essd-8-297-2016

Praetorius, S. K., Mix, A. C., Walczak, M. H., Wolhowe, M. D., Addison, J. A., & Prahl, F. G. (2015). North Pacific deglacial hypoxic events linked to abrupt ocean warming. *Nature*, *527*(7578), 362–366. https://doi.org/10.1038/nature15753

Roberts, A. P., Pike, C. R., & Verosub, K. L. (2000). First-order reversal curve diagrams: A new tool for characterizing the magnetic properties of natural samples. *Journal of Geophysical Research*, *105*(B12), 28461–28475. https://doi.org/10.1029/2000JB900326

Rustic, G. T., Koutavas, A., Marchitto, T. M., & Linsley, B. K. (2015). Dynamical excitation of the tropical Pacific Ocean and ENSO variability by little ice age cooling. *Science*, *350*(6267), 1537–1541. https://doi.org/10.1126/science.aac9937

Stoll, H. M., Vance, D., & Arevalos, A. (2007). Records of the Nd isotope composition of seawater from the Bay of Bengal: Implications for the impact of northern hemisphere cooling on ITCZ movement. *Earth and Planetary Science Letters*, *255*(1–2), 213–228. https://doi.org/10.1016/j.epsl.2006.12.016

Wang, A., Yao, Z., Dong, Z., Shi, X., Liu, Y., Gorbarenko, S., et al. (2025). Extremely depleted radiocarbon impact on estimation of glacial north Pacific intermediate water ventilation. *Earth and Planetary Science Letters*, *655*, 119254. https://doi.org/10.1016/j.epsl.2025.119254

Wang, A., Yao, Z., Shi, X., Wang, K., Zou, J., Liu, Y., et al. (2021). Orbital and millennial variations in Sea ice in the Southwestern okhotsk Sea since the last interglacial period and their implications. *Frontiers in Earth Science*, *9*, 710797. https://doi.org/10.3389/feart.2021.710797

Wang, Q., Zou, J., Feng, X., Cui, Y., Dou, R., Dong, Z., et al. (2025). Spatial variations in sedimentary fluxes and paleoenvironment in the Sea of Okhotsk over the last 30 kyr. *Quaternary Science Reviews*, *355*, 109251. https://doi.org/10.1016/j.quascirev.2025.109251

Yang, W., Zheng, H., Wang, K., Xie, X., Chen, G., & Mei, X. (2008). Sedimentary characteristics of terrigenous debris at site MD05-2905 in the northeastern part of the South China Sea since 36 ka and evolution of the East Asian monsoon. *Frontiers of Earth Science in China*, *2*(2), 170–176. https://doi.org/10.1007/s11707-008-0035-8

19448007, 2026, 18, Downloaded from https://agupubs.onlinelibrary.wiley.com/doi/10.1029/2026GL124170 by Indian Institute Of Technology, Wiley Online Library on [27/09/2026]. See the Terms and Conditions (https://onlinelibrary.wiley.com/terms-and-conditions) on Wiley Online Library for rules of use; OA articles are governed by the applicable Creative Commons License